Int J Appl Earth Obs Geoinformation 89 (2020) 102060

Contents lists available at ScienceDirect

Int J Appl Earth Obs Geoinformation

journal homepage: www.elsevier.com/locate/jag

Roles of horizontal and vertical tree canopy structure in mitigating daytime and nighttime urban heat island effects

Jike Chen[a,b], Shuangen Jin[b,c,*], Peijun Du[d]

[a] Key Laboratory of Meteorological Disaster Ministry of Education (KLME)/Joint International Research Laboratory of Climate and Environment Change (ILCEC)/ Collaborative Innovation Center on Forecast and Evaluation of Meteorological Disasters (CIC-FEMD), Nanjing University of Information Science and Technology, Nanjing 210044, China

[b] School of Remote Sensing and Geomatics Engineering, Nanjing University of Information Science and Technology, Nanjing 210044, China

[c] Shanghai Astronomical Observatory, Chinese Academy of Sciences, Shanghai 200030, China

[d] Key Laboratory for Land Satellite Remote Sensing Applications of Ministry of Natural Resources, Nanjing University, Nanjing 210093, China

ARTICLE INFO

Keywords:
Land surface temperature
Urban tree canopy
Vertical structure
Landscape pattern
Variable importance

ABSTRACT

The urban heat island (UHI) is increasingly recognized as a serious, worldwide problem because of urbanization and climate change. Urban vegetation is capable of alleviating UHI and improving urban environment by shading together with evapotranspiration. While the impacts of abundance and spatial configuration of vegetation on land surface temperature (LST) have been widely examined, very little attention has been paid to the role of vertical structure of vegetation in regulating LST. In this study, we investigated the relationships between horizontal/vertical structure characteristics of urban tree canopy and LST as well as diurnal divergence in Nanjing City, China, with the help of high resolution vegetation map, Light Detection and Ranging (LiDAR) data and various statistical analysis methods. The results indicated that composition, configuration and vertical structure of tree canopy were all significantly related to both daytime LST and nighttime LST. Tree canopy showed stronger influence on LST during the day than at night. Note that the contribution of composition of tree canopy to explaining spatial heterogeneity of LST, regardless of day and night, was the highest, followed by vertical structure and configuration. Combining composition, configuration and vertical structure of tree canopy can take advantage of their respective advantages, and best explain variation in both daytime LST and nighttime LST. As for the independent importance of factors affecting spatial variation of LST, percent cover of tree canopy (PLAND), mean tree canopy height (TH_Mean), amplitude of tree canopy height (TA) and patch cohesion index (COHESION) were the most influential during the day, while the most important variables were PLAND, maximum height of tree canopy (TH_Max), variance of tree canopy height (TH_SD) and COHESION at night. This research extends our understanding of the impacts of urban trees on the UHI effect from the horizontal to three-dimensional space. In addition, it may offer sustainable and effective strategies for urban designers and planners to cope with increasing temperature.

1. Introduction

The world has experienced rapid population growth and urbanization in past decades (Nations, 2014). Urbanization, as one of the most obvious human impacts on the earth's environment, causes the replacement of a huge amount of natural surface with impervious surface, produces the corresponding new coupled human-natural ecosystem, and triggers a variety of negative influences on urban environment (e.g., Huang and Jin, 2019). One of the most negative effects is the widely known urban heat island (UHI) effect, which is a result of increased anthropogenic heat and thermal capacity together with decreased evapotranspiration (Oke, 1973, 1982; Weng et al., 2008). The UHI effect depicts the phenomenon that urban areas experiences higher temperature compared to its surrounding non-urban area. The UHI effect not only adversely affects human health and well-being (Loughner et al., 2012; O'Loughlin et al., 2012), but also leads to increased energy consumption and air pollution (Wan et al., 2012; Grimm et al., 2008). As a result, considerable attention has been concentrated on understanding the driving factors of the UHI effect, in order to ameliorate UHI intensity, especially under the global climate warming (Wang

* Corresponding author at: School of Remote Sensing and Geomatics Engineering, Nanjing University of Information Science and Technology, Nanjing 210044, China.

E-mail address: sgjin@shao.ac.cn (S. Jin).

https://doi.org/10.1016/j.jag.2020.102060
Received 26 July 2019; Received in revised form 25 December 2019; Accepted 14 January 2020

et al., 2019; Buyantuyev and Wu, 2010).

Regarding the techniques to measure the temperature (e.g., Jin et al., 2019 and 2020), studies related to the UHI effect can be mainly grouped into two classes. Some studies were carried out to study UHI depending on air temperature (Hamdi and Schayes, 2008), while the other studies utilized remote sensing data to derive land surface temperature (LST) for evaluating the impact of UHI (Rao, 1972; Yin et al., 2018). Air temperature, which is always acquired from meteorological station, has high temporal resolution, but fails to offer a synchronized view of a large-scale area (Weng, 2009). By contrast, remote sensing techniques can provide the spatially continuous LST, and enable to link LST to ground cover characteristics in both lateral and vertical dimension. Therefore, a series of satellite and airborne remote sensing data, such as Terra/Auqa Moderate Resolution Imaging Spectroradiometer (MODIS), Landsat Thematic Mapper (TM)/Enhanced Thematic Mapper (ETM+) and Advanced Spaceborne Thermal Emission and Reflection Radiometer (ASTER), have been commonly employed to associate a wide range of factors with LST (Peng et al., 2018; Li and Zhou, 2019). In particular, the availability of high resolution imagery provides an important opportunity to distinguish the detailed information of urban land cover classes, promoting the exploration of the relationship between landscape pattern of land cover and the UHI effect.

Two fundamental aspects (i.e., composition and configuration) were used to describe landscape pattern. Composition measures the features related to the variety and relative abundance of land cover types, whereas configuration refers to the spatial characteristics and arrangement, position, or orientation of land cover types (e.g., shape complexity, aggregation and connectivity) (McGarigal, 2014). Numerous previous studies have linked land cover composition to its impacts on LST, especially for vegetation. It is consistently acknowledged that increasing vegetation cover is an very effective way to lower LST (Weng et al., 2004; Yuan and Bauer, 2007). For example, Kong et al. (2014) argued that a 10% increase in forest-vegetation cover can give rise to the decrease of LST with about 0.83 °C (Kong et al., 2014b). In addition to the total quantity of vegetation, recent studies have been undertaken to address how to optimize the landscape configuration of vegetation to enhance its cooling effect, considering the limited space to increase vegetation cover in the urban area (Li et al., 2012; Zheng et al., 2014; Guo et al., 2019). A considerable number of researchers have documented that configuration of vegetation was an important determinant of LST, because configuration of vegetation not only affects energy flows, but also has major influence on the efficiency of evapotranspiration (Edokossi et al., 2020; Calabia et al., 2020; Song et al., 2014; Huang and Wang, 2019). For instance, according to the study conducted in Sacramento, California, USA, higher edge density might amplify UHI intensity, whereas higher mean patch size seemed to reduce the impacts of UHI (Zhou et al., 2017).

Despite urban vegetation has been increasingly identified as an optimal option for alleviating the UHI effect, the research to date has tended to rely on horizontal structure of vegetation rather than three-dimensional characteristics of vegetation. It is important to stress that nascent studies have demonstrated that the cooling characteristics (i.e., shading and evapotranspiration) was more correlated with the vertical structure information of vegetation such as tree height and canopy geometry, when compared to its surface (Shahidan et al., 2010, 2012). There exist only little research that attempt to clarify the influence of vertical structure information of vegetation on LST (Kong et al., 2016; Gage and Cooper, 2017). A study conducted in Tampa, Florida, USA have revealed that vegetation height played a crucial role in regulating the daytime UHI effect. According to Davis et al. (2016), vegetation volume was an important factor impacting nighttime temperature. However, some vertical structure parameters of vegetation such as amplitude of tree height have not been examined yet. Furthermore, there is a limited knowledge exploring the relative importance of vertical structure of tree canopy compared to composition and configuration. What is not yet clear is that the extent to which variation of LST can be explained by combining landscape pattern and vertical structure of vegetation. It can be summarized that there is a need to clearly illustrate the response of vertical structure of vegetation to LST.

Using Nanjing city (China) as a case study, this study aims at a deeper understanding of the impacts of landscape pattern and vertical structure of tree canopy on the spatial variation of LST. The study was conducted on both daytime and nighttime LST, given the diurnal existence of the UHI effect (Mathew et al., 2018; Zhou et al., 2016). The key objectives of this research were presented as follows: (1) to analyze the individual and combined impact of composition, configuration and vertical structure of tree canopy on LST; (2) to assess the relative importance of influencing factors in explaining the variation of LST as well as diurnal contrast. This objective consisted of two parts. The first part was to compare the relative importance of different groups of variables, and the second part aimed to identify the dominant driving factor in terms of individual explanatory variable. Results from this study can offer important insights into whether three-dimensional nature or landscape pattern of tree canopy can have greater effects on LST, providing some effective suggestions for urban designers and planners to alleviate the influence of urbanization on the UHI.

2. Study area

Nanjing city, the capital of Jiangsu province in china, is situated in the west part of Yangtze River Delta region, and has a total population more than 8.2 million in 2016 (Nanjing, 2016). The city is characterized by the humid subtropical climate with four distinct seasons and annual average precipitation of 1033 mm. Its annual mean temperature is about 15.9 °C, with monthly average temperature ranging from 2.2 °C in January to 28.6 °C in July. The elevation of Nanjing ranges from −19 to 448 m above the mean sea level, and the topography is composed of low mountains, hills, plain and rivers (Kong et al., 2014b). The dominant tree species in this region focus on *Platanus acerifolia*, *Juiperus chinensis* and *Ligustrum lucidum* (Jim and Chen, 2003). Study area in this work, which covers an area of 204 km^2 (118°42′28″ E–118°54′29″ E, 32°2′40″–32°7′7″ N), was confined in the central part of Nanjing for two major reasons (Fig. 1). On one hand, since this study is devoted to revealing the effect of urban tree canopy on the LST, only the urbanized area was employed to minimize the bias arising from the rural area. On the other hand, the availability of airborne LiDAR data was considered.

3. Materials and methods

3.1. Land surface temperature data

Landsat data, Moderate Resolution Imaging Spectroradiometer (MODIS) LST product and ASTER images were the most widely used remote sensing data in UHI studies (Zhou et al., 2019; Deilami et al., 2018). It should be noted that Landsat data failed to provide nighttime LST, and the advantages of MODIS LST may be compromised due to low spatial resolution, although daytime LST and nighttime LST were available from MODIS LST. Therefore, given that the key objective of this study was to explore the impacts of horizontal and vertical structures of urban tree canopy on daytime LST and nighttime LST, ASTER land surface kinetic temperature product (AST_08) was employed to map daytime and nighttime LST of the study area, which is the level-2 data product at 90 m spatial resolution. AST_08 is derived from the five thermal infrared bands, with the wavelength range of 8.125–8.475, 8.475–8.825, 8.925–9.275, 10.25–10.95, 10.95–11.65 μm, respectively (Yamaguchi et al., 1998). The absolute accuracy of AST_08 was within about ±1.5 K in terms of product description (Abrams, 2000; Zheng et al., 2014).

To make the acquisition time of ASTER LST closer to the date of airborne LiDAR and tree canopy data, we have thoroughly searched LST product from 2009 to 2011. In consequence, according to the quality

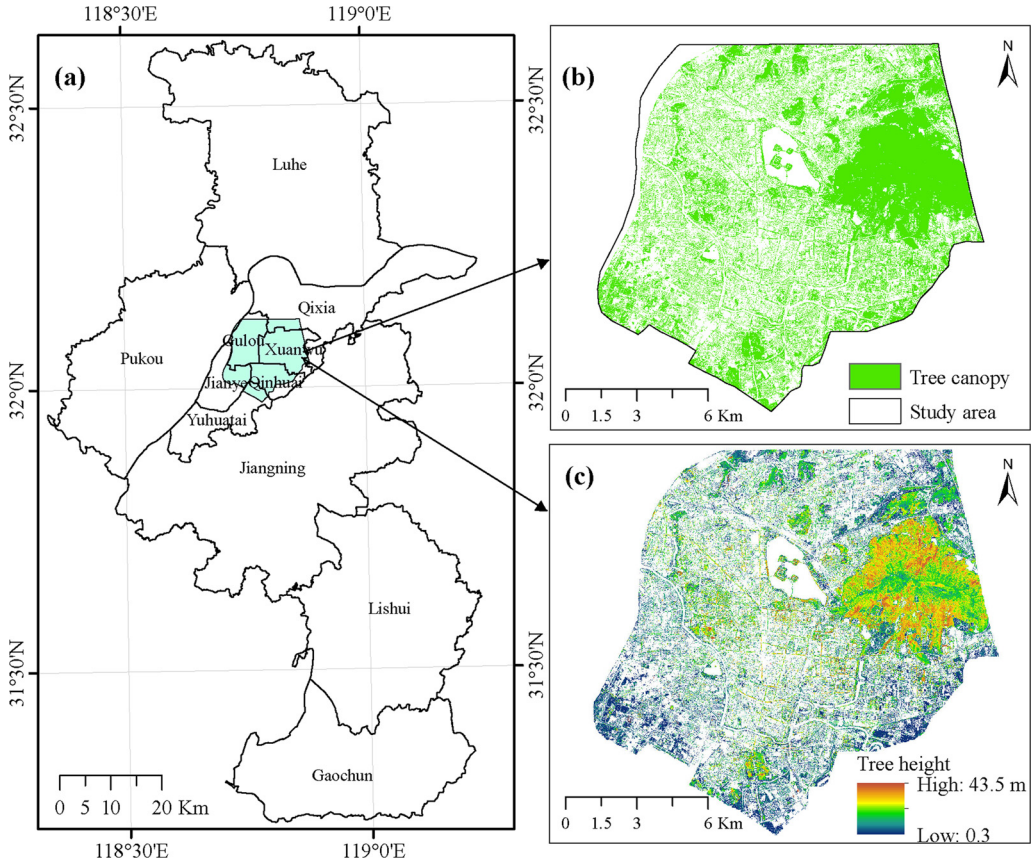

Fig. 1. Study area. (a) Location of central Nanjing, Jiangsu, China; (b) and (c) are the spatial characteristic of urban tree canopy and tree canopy height, respectively.

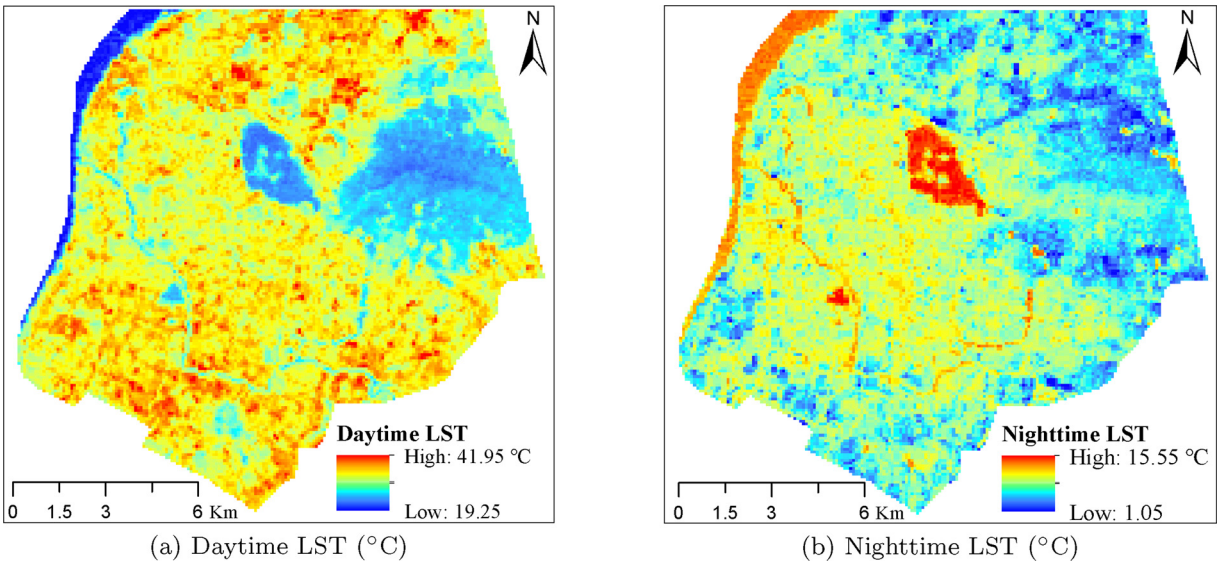

Fig. 2. LST images obtained from ASTER satellite data for daytime (May 1, 2011) (a) and nighttime (April 4, 2011) (b).

and availability of images, two ASTER LST scenes were used to analysze diurnal LST: one was obtained during daytime on May 1, 2011; the other was captured during nighttime on April 4, 2011. For the following LST analysis, We converted surface kinetic temperature to surface temperature in degree Celsius, which are displayed in Fig. 2.

3.2. Measures of composition and configuration of tree canopy

Urban tree canopy was extracted from the vegetation map with a 2-m spatial resolution, which was produced by Nanjing University and Nanjing Institute of Surveying, Mapping & Geotechnical Investigation in 2009. Based on an object-based classification method, vegetation map was achieved from the WorldView-2 satellite image on October 25, 2009, combined with ground reference and the WorldView-1 images (December 06, 2018). Detailed visual inspection and manual correction were applied to further improve the performance of vegetation map. Result revealed that the overall accuracy of vegetation map was 95.6%. Height information can be used as the criterion to differentiate tree/

shrub (i.e., tree canopy) from the vegetation, since grass is closer to the ground compared to tree/shrub. Height information of vegetation was derived from normalized Digital Surface Model (nDSM), which can be provided more detailed description in Section 3.3. According to the previous studies (Chen et al., 2009; Ucar et al., 2018), a threshold value of height was set to 0.3 in order to clearly distinguish tree/shrub objects from vegetated area in this work. Next the urban tree canopy map was improved by manual inspection, combined with ground reference and high-spatial-resolution image from Google Earth in 2009. As a result, the spatial characteristics of urban tree canopy is presented in Fig. 1(b). Furthermore, it needs to be noted that the difference between acquisition time of ASTER LST and tree canopy and LiDAR data was approximately two years. We assumed that limited change was observed as the patches of tree canopy has been relatively stable.

Many previous research have demonstrated the correlation between landscape pattern of land cover types and LST (Weng et al., 2007; Kong et al., 2014a; Zheng et al., 2014; Masoudi and Tan, 2019). Landscape metrics to quantify landscape pattern can be categorized into two main types, namely landscape composition (e.g., proportional abundance of each type) and landscape configuration (spatial arrangement of land cover types). A set of class-level landscape metrics were used to explain the variation of LST, including percent cover of tree canopy (PLAND) (Kong et al., 2014a; Zhou et al., 2017; Chen and Yu, 2017), patch density (PD) (Liu and Weng, 2009; Connors et al., 2013), edge density (ED) (Li et al., 2011; Peng et al., 2018), mean patch shape index (SHAPE_MN) (Li and Zhou, 2019; Li et al., 2012) and patch cohesion index (COHESION) (Huang and Wang, 2019). The first metric is the measure of landscape composition, whereas the latter four metrics are indicators of landscape configuration. These landscape metrics were chosen according to the following principles: (1) commonly used in previous research; (2) applicability and (3) reasonable theoretical behavior (Chen et al., 2014; Zhou et al., 2017; Fan et al., 2019).

In the analysis, the entire urban tree canopy of Nanjing was divided into 90 m × 90 m grids. All the selected metrics in class-level for each grid were computed based on the map of urban tree canopy, using the Fragstats 4.2 with the setting of 8 cell neighborhood rule. As far as Fragstats 4.2 is concerned, it is a spatial pattern analysis program, used for quantifying the composition and configuration of landscapes. Table 1 presents the definitions and formulas for landscape metrics adopted in this research.

3.3. Quantification of vertical structures regarding to tree canopy

The vertical structures of urban tree canopy were acquired by summarizing the tree canopy map as well as height information of trees into the same spatial resolution of the ASTER LST (90 m). The height of tree canopy was extracted with the aid of airborne laser scanning data, which was recorded by Optech ALTM Gemini Scanner on April 21 and 22, 2009 with the mean point density of 4.1 point/m^2 and up to four returns. We employed 2D grid cell with 2.0 m spatial resolution to process the LiDAR point cloud data, hence, 16.4 points was included for each pixel. First, identified overlap and noisy points were removed from the original LiDAR data, and then the point cloud data was subdivided into ground and no-ground points. Secondly, raster layer for height of bare earth surface (Digital Elevation Model (DEM)) was yielded from a triangular irregular network of the ground points. By computing the maximum height of all points, including ground and no-ground points, per pixel, a Digital Surface Model (DSM) was created. Finally, subtraction of DEM from the acquired DSM generated the normalized Digital Surface Model (nDSM), which denotes the height of above-ground surface objects.

The achieved tree canopy map, DSM and nDSM enabled the extraction of 3D characteristics of urban tree canopy. An overview of metrics adopted in this research, along with mathematical equations, is shown in Table 2. As can be seen from the table above, 6 vertical structure variables were calculated. To better understand how vertical structure responses to daytime LST and nighttime LST, all factors were summarized on the basis of ASTER pixel of 90 m × 90 m. The selection of these variables was not confined to the metrics that have shown significant impact on LST (e.g., TH_Mean, TH_SD) (Yu et al., 2018; Gage and Cooper, 2017). Some indicators, which may have potential influences on LST but there is lack of adequate exploration linking such indicators with LST, were also considered.

3.4. Statistical analysis

To explore how urban tree canopy influences daytime LST and nighttime LST, diurnal LST was used as the response variable in this study, while the explanatory variables were divided into three groups: composition of tree canopy, configuration of tree canopy and vertical structure of tree canopy.

A number of statistical techniques were conducted. First, in order to statistically eliminate the impacts of other influencing factors, we applied a partial correlation analysis to examine the degree of correlation between diurnal LST and predictor variables, after controlling for the mutual effect among them (Peng et al., 2013; Zhang and Liang, 2018). For instance, when we measured the linkage between diurnal LST and composition, configuration and vertical structure should be controlled for.

Next, seven stepwise multiple linear regression models were built and compared, and the diurnal LST can be expressed as a function of: (1) composition, (2) configuration, (3) vertical structure, (4) composition + configuration, (5) composition + vertical structure, (6) configuration + vertical structure and (7) composition + configuration + vertical structure. Explanatory factors with statistically significant ($p < 0.05$) were chosen for each regression model. Moreover, the change in R^2 was evaluated to investigate if the explained variation can be improved significantly by adding driving factors to base

Table 1
List of landscape metrics selected in this research to assess the composition and configuration of urban tree canopy (McGarigal, 2002).

Categories	Metrics (abbreviation)	Definition	Formulas (unit)
Composition	Percent cover of tree canopy (PLAND)	Proportional abundance of tree canopy within the spatial unit.	$PLAND_i = \frac{\sum_{j=1}^{n} a_j}{A} \times 100$ (%)
Configuration	Patch density (PD)	Density of tree canopy patches within the spatial unit.	$PD_i = \frac{n}{A} \times 10,000 \times 100$ (n/km^2)
	Edge density (ED)	The sum of edge lengths of tree canopy patches per hectare within the spatial unit.	$ED_i = \frac{\sum_{j=1}^{n} e_j}{A} \times 10,000$ (m/ha)
	Mean patch shape index (SHAPE_MN)	The average value of shape index in terms of tree canopy patches within the spatial unit.	$SHAPE\_MN_i = \frac{1}{n}\sum_{j=1}^{n} \frac{p_j}{4\sqrt{a_j}}$
	Patch cohesion index (COHESION)	Measures the physical connectedness for patches of tree canopy within the spatial unit.	$COHESION_i = \left[1 - \frac{\sum_{j=1}^{n} p_j^*}{\sum_{j=1}^{n} p_j^* \sqrt{a_j^*}}\right] \times \left[1 - \frac{1}{\sqrt{Z}}\right] \times 100$

A = area of the spatial unit; n = number of tree canopy patches within the spatial unit; e_j = lengths of edge segments of tree canopy patch j; P_j = perimeter of tree canopy patch j; a_j = area of tree canopy patch j; P_j^* = perimeter of tree canopy j regarding the number of cell surfaces; a_j^* = area of tree canopy patch j with respect to number of cells; Z = total number of cells within the spatial unit.

Table 2
Information on factors used to quantify the vertical structure of urban tree canopy in this study.

Metrics (abbreviation)	Description	Equations
Mean tree height (TH_Mean)	Mean of LiDAR-derived tree canopy height within an analysis grid	$TH\_Mean_i = \frac{\sum_{k=1}^{n} TH_k}{n}$
Maximum height of tree canopy (TH_Max)	Maximum of LiDAR-derived tree canopy height within an analysis grid.	$TH\_Max_i = Max(TH_k), j = 1, 2, 3, ..., n$
Variance of tree canopy height (TH_SD)	Standard deviation of LiDAR-derived tree canopy height within an analysis grid.	$TH\_SD_i = \sqrt{\frac{\sum_{j=1}^{n}(TH_k - TH\_mean_i)^2}{n}}$
Amplitude of tree canopy height (TA)	The difference between maximum and minimum of LiDAR-derived tree canopy height with the addition of ground elevation within an analysis grid.	$TA_i = h_{max} - h_{min}$
Normalized tree canopy height variance (NTH_SD)	The ratio between variance and mean in terms of LiDAR-derived tree canopy height within an analysis grid, a measure of relative variance of tree canopy height.	$NTH\_SD_i = \frac{TH\_SD_i}{TH\_Mean_i}$

TH_k = tree canopy height computed for cell k within the analysis unit i; h_{max} and h_{min} denote the maximum and minimum height of tree canopy within in the analysis unit i in terms of DSM, respectively.

regression models (Weinberg and Abramowitz, 2016; Li et al., 2016).

Finally, we implemented all-subsets regression to select the best subset of predictor variables. This can be attributed to the limitation of stepwise multiple linear regression that it fails to consider all potential combinations of the predictor variables, although an optimal regression model is likely to be gained. All-subset regression was implemented using "leaps" package in R, and the adjusted R^2 and Schwartz's Bayesian information criterion (BIC) (Schwarz et al., 1978) were combined to choose the optimal model. When we achieved the best subset of factors, we shed light on the relative importance of driving factors to diurnal LST, with the use of variation partitioning and hierarchical partitioning analysis. Note that variation partitioning analysis was used to identify the relative variations in diurnal LST explained by these three groups of driving factors, while hierarchical partitioning analysis was employed to quantify the relative magnitude of individual predictor variables in explaining diurnal LST variation. In this study, variation partitioning consists in apportioning the spatial variation of diurnal LST among composition, configuration and vertical structure. With three types of explanatory variables, the variation of diurnal LST were summarized into four main components: (1) the fractions independently explained by each type of explanatory variables, (2) combined fractions between two types of explanatory variables, (3) the joint fraction between all three types of explanatory variables, and (4) the unexplained variation. They were executed using the "vegan" and "hier.part" packages in statistical software R, which is widely employed among data miners for data analysis.

4. Results and analysis

4.1. The spatial and vertical characteristics of tree canopy and diurnal LST pattern

Tree canopy area was 82.4 km^2, which comprised approximately 40.3% of the study area. The mean percent cover of tree canopy (PLAND) was 44.04%, ranging from 0.05% to 100%, and varied largely in space among the analysis units in the study area (Table 3). What can clearly be seen from the table, large variations and ranges were presented for patch density and edge density of tree canopy, while mean patch shape index and patch cohesion index of tree canopy showed relatively low variation.

As regards vertical structure of tree canopy, the overall average values of mean and maximum tree canopy height were 7.39 and 21.44 m, respectively. Locations with higher tree canopy height was mostly in the eastern portion of the study area, where the Purple Mountain is located (Fig. 1(c)). The mean value of variance of tree canopy height was 4.55 m, whereas the mean value of maximum height of tree canopy was 21.44 m. When the ground elevation was considered to vertical characteristics of tree canopy (i.e., TA), TA had higher values of mean and variation compared to the other vertical structure variables.

Table 3
Descriptive statistics of diurnal LST and its driving factors.

Categories	Variables	Mean	SD	Minimum	Maximum
LST	Daytime LST	30.25	3.00	21.65	41.95
	Nighttime LST	9.00	1.67	1.25	15.25
Composition	PLAND	44.04	29.59	0.05	100.00
Configuration	PD	986.22	766.27	123.46	8271.60
	ED	871.33	534.32	0.00	3627.16
	SHAPE_MN	1.58	0.46	1.00	7.09
	COHESION	93.72	7.73	0.00	100.00
Vertical Structure	TH_Max	21.44	7.97	0.30	43.50
	TH_Mean	7.39	4.46	0.30	39.78
	TH_SD	4.55	1.96	0.00	18.41
	TA	24.77	10.68	0.00	88.20
	NTH_SD	0.77	0.38	0.00	3.61

Land surface temperature exhibited significant difference between daytime and nighttime (Fig. 2). The LST during the day ranged from 21.65 to 41.95 °C, with an average of 30.25 °C and standard deviation of 3.0 °C. On the other hand, the mean and standard deviation of LST during the night were 9.0 and 1.67 °C, respectively, ranging from 1.25 to 15.25 °C. Looking at the Figs. 1(b) and 2, it is apparent that high LST during the night was concentrated in the central region, while the high LST during the day was mainly distributed in the southern and northern regions. Further investigation argued that the higher the percent of tree canopy cover, the lower the LST for both daytime and nighttime.

4.2. Correlation between landscape pattern and vertical structure of trees and diurnal LST

We first examined the apparent response of percent cover of tree canopy to diurnal LST, with partial correlation analysis to remove the influences of configuration and vertical structure. Percent cover of tree canopy was significantly and negatively associated with both daytime LST and nighttime LST, implying that the much higher the percent cover of tree canopy, the lower the LST (Table 4).

When bivariate relationships between configuration metrics and diurnal LST were controlled with partial correlation analysis for influences of composition and vertical structure, ED, SHAPE_MN and COHESION were positively correlated with daytime LST (Table 4). However, PD was no longer correlated to daytime LST as compared to the result provided by Pearson correlation. During the night, PD and ED were negatively correlated with nighttime LST, whereas the remaining metrics showed positive associations with nighttime LST.

In the case of vertical structure variables, the Pearson correlation analysis revealed that all 5 metrics were significantly correlated with daytime LST (Table 5). When the impacts of composition and configuration of tree canopy were removed in the partial correlation, the relationship of all vertical structure metrics remained significant with daytime LST. The correlation between NTH_SD and daytime LST was

Table 4
Correlation coefficients between landscape pattern of tree canopy and diurnal LST. The results of partial correlation analysis are marked in bold and italic. As for PLAND, configuration and vertical structure of tree canopy were the control variables. PLAND and vertical structure were the control variables regarding the configuration metrics.

LST	PLAND	PD	ED	SHAPE_MN	COHESION
Daytime LST	***−0.337*** **	***−0.002***	***0.091*** **	***0.058*** **	***0.072*** **
	−0.658*	0.359**	0.330**	0.163**	−0.365**
Nighttime LST	***−0.318*** **	***−0.147*** **	***−0.048*** **	***0.076*** **	***0.067*** **
	−0.382**	0.079**	0.005	0.000	−0.196**

* Denotes the significance of correlation at 0.05 level (two-tailed).
** Denotes the significance of correlation at 0.01 level (two-tailed).

Table 5
Correlations of diurnal LST with vertical structure of tree canopy. The bold and italic rows are the partial correlation coefficients between vertical structure and diurnal LST when controlling for the composition and configuration of tree canopy.

LST	TH_Max	TH_Mean	TH_SD	TA	NTH_SD
Daytime LST	***−0.079*** **	***−0.181*** **	***−0.053*** **	***−0.165*** **	***0.085*** **
	−0.136**	−0.514**	0.042**	−0.445**	0.391**
Nighttime LST	***0.257*** **	***0.179*** **	***0.224*** **	***0.209*** **	***−0.029*** **
	0.192**	−0.031**	0.240**	−0.003	0.089**

** Denotes the significance of correlation at 0.01 level (two-tailed).

positive but negative for the others. However, it is interesting that, as for most of metrics, their partial correlation coefficients were smaller than the corresponding Pearson correlation coefficients, indicating the decreasing of the strength of partial correlation.

Another important finding is that the relationship between TH_SD and daytime LST has changed from positive to negative after considering the influence of landscape pattern of tree canopy. By contrast, the results of Pearson correlation analysis showed that all vertical structure metrics except for TA were significantly correlated with nighttime LST (Fig. 5). On the other hand, after controlling for the influences of landscape pattern of tree canopy, all metrics were significantly related to nighttime LST, and four out of five metrics exerted much stronger effects on nighttime LST independent of landscape pattern. Furthermore, TH_Mean, TA and NTH_SD showed inverse trends.

4.3. Individual and combined effects of composition, configuration and vertical structure of tree canopy on LST

To explore the relationship between diurnal LST and composition, configuration and vertical structure of tree canopy, we developed seven stepwise multiple linear regression models, which are shown in Table 6 and 7. The first three regression models attempted to clarify the effect of each group of factors on diurnal LST. In contrast, the rest of regression models were aimed to gain the understanding of what level of explanatory power of diurnal LST can be acquired using the combination of different groups of factors.

During the day, models accounted for between 31% and 54% of the variation in LST (Table 6). The best model was achieved when jointly considering composition, configuration and vertical structure as predictor variables. Configuration as a lone variables predicted the lowest amount of variation (31%) in daytime LST. The model with only vertical structure variables generated higher explanatory power (R^2), compared to models based on only composition or configuration variables.

The incremental R^2 test implied that all added variables can give rise to improvement in explaining the daytime LST variation significantly ($p < 0.001$) (Table 8). Closer inspection of this table showed that composition and vertical structure had much stronger relationships with daytime LST than did configuration. It is clearly supported by the larger R^2 increment gained by models with the addition of composition or vertical structure variables and relatively low increment of R^2 obtained by models when configuration variables were added.

In terms of land surface temperature during the night, the model with only configuration variables merely explained 4% of variation in LST (Table 7). By contrast, the three groups of predictor variables considered together accounted for the highest portion (23%) of nighttime LST's spatial variation. Adding vertical structure variables, such as mean tree canopy height and amplitude of tree canopy height, to the composition model and configuration model led to improvements of the mean prediction by 6.6% and 10.3%, respectively. Similar conclusion as like in the daytime LST can be drawn that all the addition of variables significantly improved the R^2, and composition and vertical structure had much stronger association with nighttime LST compared to configuration.

4.4. Dominant influencing factors for diurnal LST

4.4.1. Choosing the optimal model

When using the leap package in R to run all-subset regression, the parameter nbest was set to 1, suggesting that only one best model can be recorded for each size of independent variables. All the influencing factors were input to create all-subset regression model, as a result, ten regression models with different number of influencing factors were constructed. As can be seen from Fig. 3, there were some models with the same and highest adjusted R^2 for both daytime and nighttime LST. Therefore, with the aim of determining the best model, BIC was utilized as an another measurement, and a smaller BIC corresponded to a better regression model.

From the data in Fig. 3(a), we can conclude that, during the day, the model, whose adjust R^2 was 0.54 and the BIC was −17,611.25, was adopted as the optimal model. All explanatory variables except for SHAPE_MN entered the optimal model. Seven driving factors were contained in the best model for nighttime LST, with 0.23 and −6021.32 for adjust R^2 and BIC value, respectively (Fig. 3(b)). These factors were composed of PLAND, two configuration variables (PD and COHESION),

Table 6
Summary results, including regression coefficients and determination coefficients (R^2), for seven stepwise multiple linear regressions by using daytime LST as the response variable.

Model	Composition	Configuration				Vertical Structure					R^2
	PLAND	PD	ED	SHAPE_MN	COHESION	TH_Max	TH_Mean	TH_SD	TA	NTH_SD	
Model 1	−0.066										0.43
Model 2		4.91E−04	0.001	1.142	−0.159						0.31
Model 3						0.121	−0.440	0.478	−0.142	−1.585	0.45
Model 4	−0.067	−3.03E−04	0.001	0.453							0.50
Model 5	−0.038					0.072	−0.277	0.259	−0.081	−0.828	0.53
Model 6		2.58E−04		−0.052		0.111	−0.397	0.421	−0.124	−1.411	0.48
Model 7	−0.046	−1.94E−04	5.63E−04	0.013		0.060	−0.226	0.199	−0.070	−0.764	0.54

Table 7
Summary results, including regression coefficients and determination coefficients (R^2), for seven stepwise multiple linear regressions by using nighttime LST as the response variable.

Model	Composition	Configuration				Vertical Structure					R^2
	PLAND	PD	ED	SHAPE_MN	COHESION	TH_Max	TH_Mean	TH_SD	TA	NTH_SD	
Model 1	−0.022										0.15
Model 2		5.20E−05		0.200	−0.043						0.04
Model 3						0.075	−0.122	0.207	−0.037	−1.036	0.12
Model 4	−0.031	−3.37E−04		−0.145	0.028						0.17
Model 5	−0.024					0.046	−0.021	0.070		−0.568	0.21
Model 6		−6.70E−05	−2.57E−04	−0.031		0.075	−0.128	0.212	−0.031	−0.908	0.15
Model 7	−0.031	−3.53E−04	6.90E−05	0.015		0.041	−0.016	0.066	0.004	−0.475	0.23

Table 8
The significance test of incremental R^2: the increase in R^2 when additional driving factors were added to base models.

Base models	Base models with the additional driving factors							
	Composition + Configuration		Composition + VS		Configuration + VS		Composition + Configuration + VS	
	Daytime	Nighttime	Daytime	Nighttime	Daytime	Nighttime	Daytime	Nighttime
Composition	0.064[a]	0.024[a]	0.097[a]	0.066[a]			0.103[a]	0.086[a]
Configuration	0.19[a]	0.129[a]			0.17[a]	0.103[a]	0.229[a]	0.191[a]
Vertical Structure (VS)			0.076[a]	0.095[a]	0.023[a]	0.029[a]	0.082[a]	0.115[a]
Composition + Configuration							0.039[a]	0.062[a]
Composition + VS							0.006[a]	0.020[a]
Configuration + VS							0.056[a]	0.086[a]

[a] Implies the statistical significance of increment in R^2 at $\alpha = 0.001$ with the F-test.

and four vertical structure variables, including TH_Max, TH_Mean, TH_SD and NTH_SD.

4.4.2. Relative importance of landscape pattern and vertical structure of tree canopy for LST

Based on the explanatory variables that survived during the optimal models, the relative contributions of landscape pattern and vertical structure of tree canopy were assessed through the use of variation partitioning and hierarchical partitioning. First, with respect to the results of variation partitioning for daytime LST (Fig. 4(a)), the joint of all three types of influencing factors contributed to a considerable amount of variation (21.37%), which accounted for approximately 40% of the explained variation. The variations of daytime LST independently explained by composition and vertical structure were 5.95% and 4.19%, respectively. However, the configuration uniquely captured very limited additional explanation of variation (0.6%) related to daytime LST. A high proportion of LST variation (14.26%) during the day can be jointly explained by composition and vertical structure, whereas the joint impact of composition and configuration made very limited contribution.

The results of variation partitioning for nighttime LST, as shown in Fig. 4(b), reported that the unique effects of composition and vertical structure variables dominated the LST variation during the night (10.07% and 6.31%, respectively).What is important for us to recognize here, is that not only the independent contribution of configuration, but also the joint effects of configuration and composition or configuration and vertical structure was found to be relatively weak. Variation of nighttime LST explained by the joint of the three types of variables was negative, signifying a few of the correlations among explanatory variables have opposite signs or the occurrence of suppression (Pedzahur, 1997).

In addition to quantifying the relative importance of each group of influencing factors, the contribution of individual explanatory variable to diurnal LST was also explored. Hierarchical partitioning analysis suggested that PLAND appeared the most important variable in accounting for the LST variation during the day (Fig. 5(a)). PD, ED and COHESION independently contributed 4.98%, 6.11% and 7.42% of the variation of daytime LST, respectively. In the case of vertical structure, TH_Mean and TA made larger independent contribution rate to the LST variation (16.59% and 14.26%, respectively), followed by NTH_SD (7.07%), TH_STD (3.14%), and TH_Max (2.86%).

During the night, the highest independent contribution rate (56.23%) to the LST variation was assigned to PLAND (Fig. 5(b)). COHESION made much larger contribution rate (9.24%) to nighttime LST variation than did PD (4.38%). TH_Max and TH_STD had the relatively higher independent contribution rate of LST variation (12.31% and 12.50%, respectively), while the contributions of NTH_STD and TH_Mean to nighttime LST were very limited.

5. Discussion

5.1. Diurnal divergence in the sensitivity of landscape pattern and vertical structure of tree canopy to LST

Akin to the results in many previous studies (Huang and Wang, 2019; Zhou et al., 2017; Peng et al., 2014), our results confirmed that percent cover of tree canopy played the most important role in cooling LST, regardless of day and night (Fig. 4 and 5). Another important finding was that percent cover of tree canopy showed stronger impact on LST during the day than at night (Table 4, 6 and 7). Such an phenomenon can be explained from the point of view of cooling mechanism with regard to tree canopy. It is acknowledged that the general cooling effect of tree canopy on LST resulted from shading and evapotranspiration, which could convert solar radiation to latent heat flux (Shahidan et al., 2012; Lambers et al., 2008; Chen et al., 2019). The reduced impact of tree canopy on LST at nighttime could be attributed to the combined effects of the following two main aspects. On one hand, during the night, evapotranspiration effect of tree canopy tended to reduce as photosynthesis shut down. On the other hand, it is likely to be explained in part by the fact that tree canopy hindered the loss of longwave radiation together with below-canopy turbulence (Ziter et al., 2019; Konarska et al., 2016).

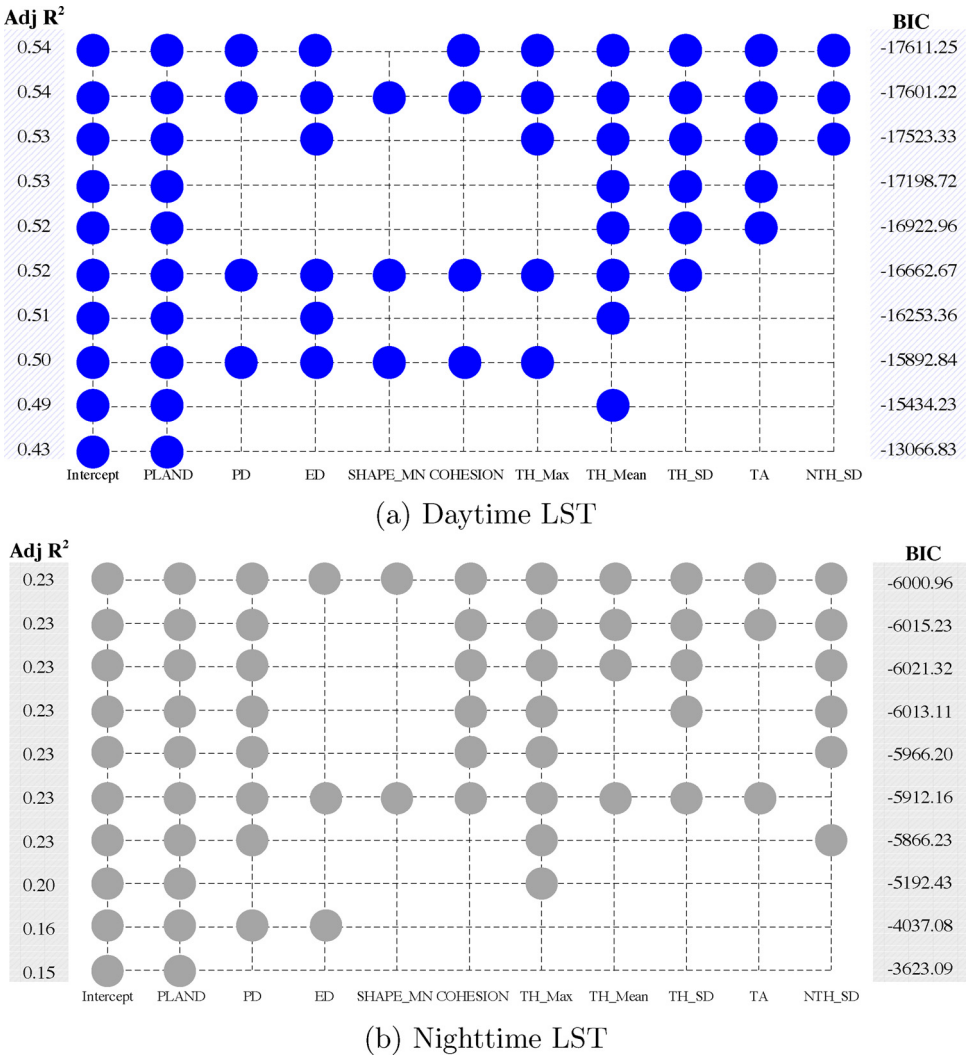

Fig. 3. All the best subset regression models for (a) daytime LST and (b) nighttime LST.

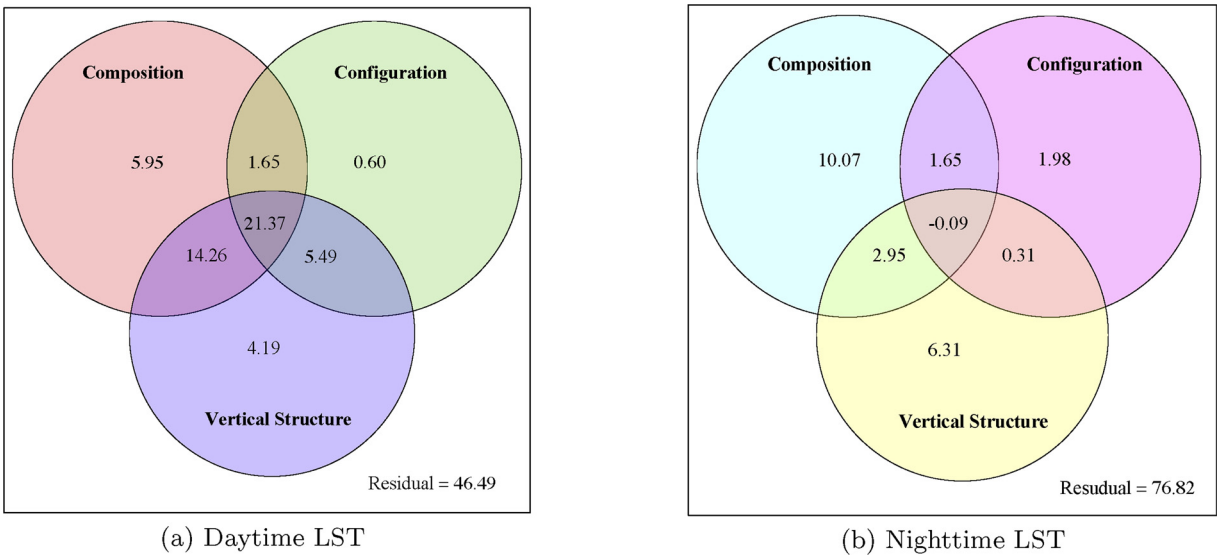

Fig. 4. The unique and joint impacts of composition, configuration and vertical structure of trees on the (a) daytime LST and (b) nighttime LST.

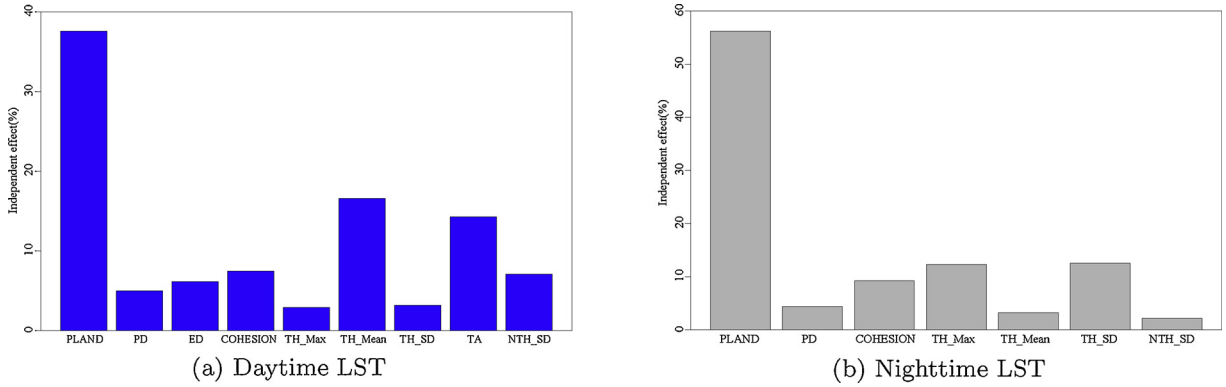

Fig. 5. The relative contribution of individual explanatory variable to (a) daytime LST and (b) nighttime LST.

In this work, we also affirmed that most of configuration metrics related to tree canopy were shown to have significant impact on both daytime LST and nighttime LST, after controlling for the impact of composition and vertical structure of tree canopy. What stands out in the Table 4 is that edge density was positively associated with daytime LST, but the inverse trend was presented for nighttime LST. As far as edge density is concerned, the increase of edge density and total patch edges tended to result in more shade produced by tree canopy, and improved the energy exchange between trees and surrounding ground surfaces such as impervious surface. Consequently, higher edge density always gave rise to lower LST in terms of shading effect. By contrast, many prior studies have proven that larger patches can lead to much stronger evapotranspiration. However, in the light of a fixed area of tree canopy cover, higher edge density suggested that patches of tree canopy was relatively more fragmented. It means that the increase in edge density perhaps reduced the evaportanspiration, which is accompanied with higher LST (Zhou et al., 2017; Cao et al., 2010). According the aforementioned information, we can conclude that, during the day, the change in LST was determined by the joint effects of shading and transpiration. Therefore, the reason why edge density was positively correlated with daytime LST is that the reduction of evapotranspiration provided by increased edge density was over increase in shading. One possible explanation for the phenomenon, which increased edge density can lead to lower nighttime LST, was that although increasing edge density maybe tended to reduce evapotranspiration efficiency, it can also increase outgoing radiation (Holmer et al., 2013).

Additionally, this study demonstrated that configuration metrics of tree canopy were weaker explanatory variables of diurnal LST, when compared to composition and vertical structure measures of tree canopy. However, it is worth noting that, similar to some previous work (Li et al., 2016; Zhou et al., 2011), combining configuration and composition (vertical structure) improved significantly the explanation of variation in LST, regardless of day and night, but only limited.

By exploring the influences of trees on LST with different spatial resolutions, which were derived from different satellite sensors, our results were in keeping with the findings of previous studies (Zhou et al., 2017; Zheng et al., 2014). For example, Zhou et al. (2017) found that percent cover of trees played a more important role in predicting LST than that of spatial configuration of trees, using the Landsat-5 Thematic Mapper with a spatial resolution of 120 m to derived LST (Zhou et al., 2017). Nastran et al. (2019) demonstrated that tree configuration and composition were statistically significantly correlated with UHI intensity under the condition of LST derived from MODIS (Nastran et al., 2019). In terms of the influences of the spatial resolution of urban tree canopy map on the relationship between trees and LST, conclusions obtained by this study supported previous research that composition and configuration of tree canopy can be both of great importance to mitigate the UHI effect, although there are some differences in the light of the relationships between configuration metrics of tree canopy and LST (Kong et al., 2014a; Fan et al., 2015).

Although the impact of vegetation on LST has been widely explored (Kong et al., 2014a; Weng et al., 2004; Yuan and Bauer, 2007), the response of vertical structure of tree canopy to LST, especially for diurnal contrast, is not fully understood. Our results indicated that all vertical structure measures in this study had significant influences on daytime LST and nighttime LST, when the influences of landscape pattern was removed. Note that the inverse trend between daytime LST and nighttime LST was observed for all vertical structure measures (Table 5). For example, we found that daytime LST decreased with increasing mean tree height, while nighttime LST tended to decrease as mean tree height increases. The contribution of vertical structure to affecting LST was close to composition, but much higher than configuration. We thought that vertical structure and landscape pattern can provide complementary information, which might explain why the integration of these influencing factors can explain more LST variation (Gage and Cooper, 2017; Davis et al., 2016; Yu et al., 2018). Regarding the independent effects of vertical structure variables, TH_Mean and TA played more important roles in explaining LST during the day, while TH_Max and TH_SD showed stronger impacts on nighttime LST.

5.2. Implications for management and urban planning

It is well known that vegetation, especially for tree canopy, played a vital role in mitigating urban heat island (Weng et al., 2004; Jiao et al., 2017; Zhou et al., 2017). Up to now, most previous studies have tended to focus on exploring how the abundance and spatial configuration of tree canopy affected the magnitude of LST. However, the contribution of vertical structure characteristics of tree canopy to impacting LST was less understood. The outcomes of this study can provide some innovative insights into urban planning and management.

Our results demonstrated that not only the abundance and configuration of tree canopy but also vertical structure of tree canopy can significantly influence LST. Though the abundance of tree canopy showed stronger impact on LST, special attention should be focused on the optimizations of configuration and vertical structure of tree canopy given the limited available land space for planting trees. As for spatial configuration of tree canopy, the stronger positive relationship between patch cohesion index (COHSEION) and LST suggested that a decrease in degree of tree canopy connectivity could produce cooling effect. It can be done by interspersing tree canopy into urban area to cool the city most efficiently, which is in line with some prior studies (Zhou et al., 2011). Apart from exploring where the trees should be planted, this study also revealed that vertical structure of trees should be considered to maximize the cooling effect of tree canopy. We excepted that the aforementioned results have important implications for urban planners and designers.

5.3. Limitations

Although we have revealed the impacts of landscape pattern and vertical structure of tree canopy on diurnal LST in this work, a number of limitations need to be considered. Firstly, ASTER LST used in this work was acquired in 2011, but the acquisition time of tree canopy and airborne LiDAR data was 2009. The time difference between these data maybe have some inevitable impacts on the results obtained in this study. As a result, in order to make our study more persuasive, it is an urgent need to compare the conclusions achieved in similar research in the future, using the data with approximately same acquisition date. Secondly, using only one daytime/nighttime LST we were capable of thoroughly unraveling how horizontal and vertical tree canopy structure influence urban thermal environment. However, whether these finding can hold true should be further explored in other cities with different climatic conditions, using multiple daytime and nighttime thermal images. Thirdly, we were not devoting to investigating the seasonal contrast in the relationship between LST and tree canopy in terms of lateral and vertical structure information. However, given that the influences of vegetation phenology on LST, the association between vegetation and LST varied with seasons (Fan et al., 2015; Zhou et al., 2014). Hence, future research might explore the seasonal impacts of tree canopy on LST to complement this work. Finally, some other vertical structure metrics such as sky view factor and canopy density may play a role but not covered in this study. Therefore, future research should be undertaken to give a better understanding of the influence of vertical structure of tree canopy on LST.

6. Conclusion

A comprehensive understanding of the cooling effect of tree canopy could extend our knowledge on how to ameliorate city's resilience to future climate change. The uniqueness of this study lies in the exploration of characteristics of tree canopy, including landscape pattern and vertical structure, on the diurnal LST variation. The findings of this work showed that tree canopy was able to explain greater amount of variation in daytime LST than in nighttime LST. Composition of tree canopy was the most important predictor in reducing LST regardless of day and night, followed by vertical structure and configuration. Note that a combination of composition, configuration and vertical structure of tree canopy can provide complementary information, and best explain the variation of LST. Furthermore, according to the contribution of individual influencing factor to LST, we found that the dominant explanatory variables were PLAND, TH_Mean, TA and COHESION during the day. By contrast, the major determinants of LST were PLAND, TH_Max, TH_SD and COHESION at night. Our results suggested that, in order to mostly effectively alleviate the UHI effect, we should not only aim at the enlargement of tree canopy area and the optimization of spatial configuration of tree canopy, but should also take the vertical structure of tree canopy into account.

Acknowledgements

This work is supported by Strategic Priority Research Program Project of the Chinese Academy of Sciences (Grant No. XDA23040100), Jiangsu Province Distinguished Professor Project (Grant No. R2018T20), Startup Foundation for Introducing Talent of NUIST (Grant No. 2243141801036), and the program B for outstanding PhD candidate of Nanjing University (No. 201701B019). We thank Wenquan Han from Nanjing Institute of Surverying, Mapping and Geotechnical Investigation for providing airborne LiDAR data. Special thanks are due to Iñigo Molina and Haiyong Ding for giving some useful suggestions and checking the writing.

References

Abrams, M., 2000. The Advanced Spaceborne Thermal Emission and Reflection Radiometer (ASTER): data products for the high spatial resolution imager on NASA's Terra platform. Int. J. Rem. Sens. 21, 847–859.
Buyantuyev, A., Wu, J., 2010. Urban heat islands and landscape heterogeneity: linking spatiotemporal variations in surface temperatures to land-cover and socioeconomic patterns. Landsc. Ecol. 25, 17–33.
Calabia, A., Molina, I., Jin, S.G., 2020. Soil moisture content from GNSS reflectometry using dielectric permittivity from fresnel reflection coefficients. Remote Sens. 12 (1), 122. https://doi.org/10.3390/rs12010122.
Cao, X., Onishi, A., Chen, J., Imura, H., 2010. Quantifying the cool island intensity of urban parks using ASTER and IKONOS data. Landsc. Urban Plan. 96, 224–231.
Chen, A., Yao, L., Sun, R., Chen, L., 2014. How many metrics are required to identify the effects of the landscape pattern on land surface temperature? Ecol. Indic. 45, 424–433.
Chen, X., Zhao, P., Hu, Y., Ouyang, L., Zhu, L., Ni, G., 2019. Canopy transpiration and its cooling effect of three urban tree species in a subtropical city-Guangzhou, China. Urban For. Urban Green. 126368.
Chen, Y., Su, W., Li, J., Sun, Z., 2009. Hierarchical object oriented classification using very high resolution imagery and LIDAR data over urban areas. Adv. Space Res. 43, 1101–1110.
Chen, Y., Yu, S., 2017. Impacts of urban landscape patterns on urban thermal variations in Guangzhou, China. Int. J. Appl. Earth Obs. Geoinf. 54, 65–71.
Connors, J.P., Galletti, C.S., Chow, W.T., 2013. Landscape configuration and urban heat island effects: assessing the relationship between landscape characteristics and land surface temperature in Phoenix, Arizona. Landsc. Ecol. 28, 271–283.
Davis, A.Y., Jung, J., Pijanowski, B.C., Minor, E.S., 2016. Combined vegetation volume and "greenness" affect urban air temperature. Appl. Geogr. 71, 106–114.
Deilami, K., Kamruzzaman, M., Liu, Y., 2018. Urban heat island effect: a systematic review of spatio-temporal factors, data, methods, and mitigation measures. Int. J. Appl. Earth Obs. Geoinf. 67, 30–42.
Edokossi, K., Calabia, A., Jin, S.G., Molina, I., 2020. GNSS-Reflectometry and Remote Sensing of Soil Moisture: a review of measurement techniques, methods and applications. Remote Sens. 12 (4), 614. https://doi.org/10.3390/rs12040614.
Fan, C., Myint, S.W., Zheng, B., 2015. Measuring the spatial arrangement of urban vegetation and its impacts on seasonal surface temperatures. Prog. Phys. Geogr. 39, 199–219.
Fan, H., Yu, Z., Yang, G., Liu, T.Y., Liu, T.Y., Hung, C.H., Vejre, H., 2019. How to cool hot-humid (Asian) cities with urban trees? An optimal landscape size perspective. Agric. For. Meteorol. 265, 338–348.
Gage, E.A., Cooper, D.J., 2017. Urban forest structure and land cover composition effects on land surface temperature in a semi-arid suburban area. Urban For. Urban Green. 28, 28–35.
Grimm, N.B., Faeth, S.H., Golubiewski, N.E., Redman, C.L., Wu, J., Bai, X., Briggs, J.M., 2008. Global change and the ecology of cities. Science 319, 756–760.
Guo, G., Wu, Z., Chen, Y., 2019. Complex mechanisms linking land surface temperature to greenspace spatial patterns: evidence from four southeastern Chinese cities. Sci. Total Environ. 674, 77–87.
Hamdi, R., Schayes, G., 2008. Sensitivity study of the urban heat island intensity to urban characteristics. Int. J. Climatol. 28, 973–982.
Holmer, B., Thorsson, S., Lindén, J., 2013. Evening evapotranspirative cooling in relation to vegetation and urban geometry in the city of Ouagadougou, Burkina Faso. Int. J. Climatol. 33, 3089–3105.
Huang, M., Jin, S.G., 2019. A methodology for simple 2-D inundation analysis in urban area using SWMM and GIS. Nat. Hazards 97 (1), 15–43. https://doi.org/10.1007/s11069-019-03623-2.
Huang, X., Wang, Y., 2019. Investigating the effects of 3D urban morphology on the surface urban heat island effect in urban functional zones by using high-resolution remote sensing data: a case study of Wuhan, central China. ISPRS J. Photogramm. Remote Sens. 152, 119–131.
Jiao, M., Zhou, W., Zheng, Z., Wang, J., Qian, Y., 2017. Patch size of trees affects its cooling effectiveness: a perspective from shading and transpiration processes. Agric. For. Meteorol. 247, 293–299.
Jim, C.Y., Chen, S.S., 2003. Comprehensive greenspace planning based on landscape ecology principles in compact Nanjing city, China. Landsc. Urban Plan. 65, 95–116.
Jin, S.G., Gao, C., Li, J., 2019. Atmospheric sounding from FY-3C GPS radio occultation observations: first results and validation. Adv. Meteorol. 2019, 1–13. https://doi.org/10.1155/2019/4780143. Article ID 4780143.
Jin, S.G., Gao, C., Li, J., 2020. Estimation and analysis of global gravity wave using GNSS radio occultation data from FY-3C meteorological satellite. J. Nanjing Univ. Infor. Sci. (Nat. Sci. Edn.) 12 (1). https://doi.org/10.13878/j.cnki.jnuist.2020.01.008.
Konarska, J., Holmer, B., Lindberg, F., Thorsson, S., 2016. Influence of vegetation and building geometry on the spatial variations of air temperature and cooling rates in a high-latitude city. Int. J. Climatol. 36, 2379–2395.
Kong, F., Yan, W., Zheng, G., Yin, H., Cavan, G., Zhan, W., Zhang, N., Cheng, L., 2016. Retrieval of three-dimensional tree canopy and shade using terrestrial laser scanning (TLS) data to analyze the cooling effect of vegetation. Agric. For. Meteorol. 217, 22–34.
Kong, F., Yin, H., James, P., Hutyra, L.R., He, H.S., 2014a. Effects of spatial pattern of greenspace on urban cooling in a large metropolitan area of eastern China. Landsc. Urban Plan. 128, 35–47.
Kong, F., Yin, H., Wang, C., Cavan, G., James, P., 2014b. A satellite image-based analysis of factors contributing to the green-space cool island intensity on a city scale. Urban For. Urban Green. 13, 846–853.

Lambers, H., Chapin III, F.S., Pons, T.L., 2008. Plant Physiological Ecology. Springer Science & Business Media.
Li, J., Song, C., Cao, L., Zhu, F., Meng, X., Wu, J., 2011. Impacts of landscape structure on surface urban heat islands: a case study of shanghai, china. Remote Sens. Environ. 115, 3249–3263.
Li, X., Li, W., Middel, A., Harlan, S., Brazel, A., Turner Ii, B., 2016. Remote sensing of the surface urban heat island and land architecture in Phoenix, Arizona: combined effects of land composition and configuration and cadastral-demographic-economic factors. Remote Sens. Environ. 174, 233–243.
Li, X., Zhou, W., 2019. Optimizing urban greenspace spatial pattern to mitigate urban heat island effects: extending understanding from local to the city scale. Urban For. Urban Green. 41, 255–263.
Li, X., Zhou, W., Ouyang, Z., Xu, W., Zheng, H., 2012. Spatial pattern of greenspace affects land surface temperature: evidence from the heavily urbanized Beijing metropolitan area, China. Landsc. Ecol. 27, 887–898.
Liu, H., Weng, Q., 2009. Scaling effect on the relationship between landscape pattern and land surface temperature. Photogramm. Eng. Remote Sens. 75, 291–304.
Loughner, C.P., Allen, D.J., Zhang, D.L., Pickering, K.E., Dickerson, R.R., Landry, L., 2012. Roles of urban tree canopy and buildings in urban heat island effects: parameterization and preliminary results. J. Appl. Meteorol. Climatol. 51, 1775–1793.
Masoudi, M., Tan, P.Y., 2019. Multi-year comparison of the effects of spatial pattern of urban green spaces on urban land surface temperature. Landsc. Urban Plan. 184, 44–58.
Mathew, A., Khandelwal, S., Kaul, N., 2018. Analysis of diurnal surface temperature variations for the assessment of surface urban heat island effect over Indian cities. Energy Build. 159, 271–295.
McGarigal, K., 2002. Fragstats: Spatial Pattern Analysis Program for Categorical Maps. Computer software program produced by the authors at the University of Massachusetts, Amherst .. http://www.umass.edu/landeco/research/fragstats/fragstats.html.
McGarigal, K., 2014. Landscape pattern metrics. Wiley StatsRef: Stat. Ref.e Online.
Nanjing, 2016. Bureau of Statistics. Nanjing Statistical Yearbook, pp. 2016.
Nastran, M., Kobal, M., Eler, K., 2019. Urban heat islands in relation to green land use in european cities. Urban For. Urban Green. 37, 33–41.
Nations, U., 2014. World Urbanization Prospects: The 2014 Revision, Highlights. Department of Economic and Social Affairs. Population Division, United Nations, pp. 32.
Oke, T.R., 1973. City size and the urban heat island. Atmos. Environ. (1967) 7, 769–779.
Oke, T.R., 1982. The energetic basis of the urban heat island. Quart. J. R. Meteorol. Soc. 108, 1–24.
O'Loughlin, J., Witmer, F.D., Linke, A.M., Laing, A., Gettelman, A., Dudhia, J., 2012. Climate variability and conflict risk in East Africa, 1990–2009. Proc. Natl. Acad. Sci. U.S.A 109, 18344–18349.
Pedzahur, E., 1997. Multiple Regression in Behavioral Research: Explanation and Prediction. Wadsworth, Thompson Learning, London, UK.
Peng, J., Jia, J., Liu, Y., Li, H., Wu, J., 2018. Seasonal contrast of the dominant factors for spatial distribution of land surface temperature in urban areas. Rem. Sens. Environ. 215, 255–267.
Peng, S., Piao, S., Ciais, P., Myneni, R.B., Chen, A., Chevallier, F., Dolman, A.J., Janssens, I.A., Penuelas, J., Zhang, G., et al., 2013. Asymmetric effects of daytime and night-time warming on northern hemisphere vegetation. Nature 501, 88.
Peng, S.S., Piao, S., Zeng, Z., Ciais, P., Zhou, L., Li, L.Z., Myneni, R.B., Yin, Y., Zeng, H., 2014. Afforestation in china cools local land surface temperature. Proc. Natl. Acad. Sci. U.S.A. 111, 2915–2919.
Rao, P.K., 1972. Remote sensing of urban "heat islands" from an environmental satellite. Bull. Am. Meteorol. Soc. 53, 647–648.
Schwarz, G., et al., 1978. Estimating the dimension of a model. Ann. Stat. 6, 461–464.
Shahidan, M.F., Jones, P.J., Gwilliam, J., Salleh, E., 2012. An evaluation of outdoor and building environment cooling achieved through combination modification of trees with ground materials. Build. Environ. 58, 245–257.
Shahidan, M.F., Shariff, M.K., Jones, P., Salleh, E., Abdullah, A.M., 2010. A comparison of *Mesua ferrea L.* and *Hura crepitans L.* for shade creation and radiation modification in improving thermal comfort. Landsc. Urban Plan. 97, 168–181.
Song, J., Du, S., Feng, X., Guo, L., 2014. The relationships between landscape compositions and land surface temperature: quantifying their resolution sensitivity with spatial regression models. Landsc. Urban Plan. 123, 145–157.
Ucar, Z., Bettinger, P., Merry, K., Akbulut, R., Siry, J., 2018. Estimation of urban woody vegetation cover using multispectral imagery and LiDAR. Urban For. Urban Green. 29, 248–260.
Wan, K.K., Li, D.H., Pan, W., Lam, J.C., 2012. Impact of climate change on building energy use in different climate zones and mitigation and adaptation implications. Appl. Energy 97, 274–282.
Wang, Y.D., Jin, S.G., Sun, X., Wang, F., 2019. Winter weather regimes in Southeastern China and its intra-seasonal variations. Atmosphere 10 (5), 271. https://doi.org/10.3390/atmos10050271.
Weinberg, S.L., Abramowitz, S.K., 2016. Statistics Using IBM SPSS: An Integrative Approach. Cambridge University Press.
Weng, Q., 2009. Thermal infrared remote sensing for urban climate and environmental studies: methods, applications, and trends. ISPRS J. Photogramm. Remote Sens. 64, 335–344.
Weng, Q., Liu, H., Liang, B., Lu, D., 2008. The spatial variations of urban land surface temperatures: pertinent factors, zoning effect, and seasonal variability. IEEE J. Sel. Top. Appl. Earth Observ. Remote Sens. 1, 154–166.
Weng, Q., Liu, H., Lu, D., 2007. Assessing the effects of land use and land cover patterns on thermal conditions using landscape metrics in city of Indianapolis, United States. Urban Ecosyst. 10, 203–219.
Weng, Q., Lu, D., Schubring, J., 2004. Estimation of land surface temperature-vegetation abundance relationship for urban heat island studies. Remote Sens. Environ. 89, 467–483.
Yamaguchi, Y., Kahle, A.B., Tsu, H., Kawakami, T., Pniel, M., 1998. Overview of advanced spaceborne thermal emission and reflection radiometer (ASTER). IEEE Trans. Geosci. Remote Sens. 36, 1062–1071.
Yin, C., Yuan, M., Lu, Y., Huang, Y., Liu, Y., 2018. Effects of urban form on the urban heat island effect based on spatial regression model. Sci. Total Environ. 634, 696–704.
Yu, Q., Acheampong, M., Pu, R., Landry, S.M., Ji, W., Dahigamuwa, T., 2018. Assessing effects of urban vegetation height on land surface temperature in the City of Tampa, Florida, USA. Int. J. Appl. Earth Obs. Geoinf. 73, 712–720.
Yuan, F., Bauer, M.E., 2007. Comparison of impervious surface area and normalized difference vegetation index as indicators of surface urban heat island effects in Landsat imagery. Remote Sens. Environ. 106, 375–386.
Zhang, Y., Liang, S., 2018. Impacts of land cover transitions on surface temperature in China based on satellite observations. Environ. Res. Lett. 13, 024010.
Zheng, B., Myint, S.W., Fan, C., 2014. Spatial configuration of anthropogenic land cover impacts on urban warming. Landsc. Urban Plan. 130, 104–111.
Zhou, D., Xiao, J., Bonafoni, S., Berger, C., Deilami, K., Zhou, Y., Frolking, S., Yao, R., Qiao, Z., Sobrino, J., 2019. Satellite remote sensing of surface urban heat islands: progress, challenges, and perspectives. Rem. Sens. 11, 48.
Zhou, D., Zhang, L., Li, D., Huang, D., Zhu, C., 2016. Climate-vegetation control on the diurnal and seasonal variations of surface urban heat islands in china. Environ. Res. Lett. 11, 074009.
Zhou, W., Huang, G., Cadenasso, M.L., 2011. Does spatial configuration matter? Understanding the effects of land cover pattern on land surface temperature in urban landscapes. Landsc. Urban Plan. 102, 54–63.
Zhou, W., Qian, Y., Li, X., Li, W., Han, L., 2014. Relationships between land cover and the surface urban heat island: seasonal variability and effects of spatial and thematic resolution of land cover data on predicting land surface temperatures. Landsc. Ecol. 29, 153–167.
Zhou, W., Wang, J., Cadenasso, M.L., 2017. Effects of the spatial configuration of trees on urban heat mitigation: a comparative study. Rem. Sens. Environ. 195, 1–12.
Ziter, C.D., Pedersen, E.J., Kucharik, C.J., Turner, M.G., 2019. Scale-dependent interactions between tree canopy cover and impervious surfaces reduce daytime urban heat during summer. Proc. Natl. Acad. Sci. U.S.A. 201817561.